J Solid State Electrochem (2001) 6: 63–68
DOI 10.1007/s100080000160

ORIGINAL PAPER

K. Arun Prasad · P. Giridhar · Visalakshi Ravindran
V.S. Muralidharan

Zinc-cobalt alloy: electrodeposition and characterization

Received: 23 December 1999 / Accepted: 6 July 2000 / Published online: 6 July 2001

Abstract Zinc-cobalt alloy electrodeposits offer enhanced corrosion protection to steel, compared to zinc deposits. A near neutral zinc-cobalt alloy sulfate bath was developed. In the absence of β-naphthol and sodium lauryl sulfate (SLS), only a light grey and non-uniform deposit was obtained. Addition of boric acid yielded a grey and uniform deposit. To obtain the grey uniform alloy deposit, the optimum bath composition was: 0.5 M $ZnSO_4$, 0.5 M $CoSO_4$, 40 g/L H_3BO_3, 0.865 g/L SLS and 0.345 g/L β-naphthol. The current efficiency for alloy deposition was 50% in the current density range 0.5–2.5 A/dm^2. X-ray fluorescence studies on the alloy deposit formed on steel revealed 58–75% zinc on the surface. Anodic stripping voltammetric studies were carried out on zinc-cobalt alloy films formed on glassy carbon to identify the phases formed in the alloy. Zn-Co alloy film dissolution peaks suggested the existence of β, β_1 and γ phases of the alloy.

Keywords Zinc-cobalt alloy · Electrodeposition · X-ray fluorescence spectroscopy

Introduction

It is a common belief that zinc offers protection to steel by sacrificing itself. Verbene [1] found contradictory results in terms of this corrosion protection. Zinc becomes passivated and the protective property is hindered. Hence development of zinc alloy coatings formed with noble metals was initiated and led to the development of Zn-Ni, Zn-Co and Zn-Fe alloy plating baths. Zinc-cobalt alloys have been electrodeposited from acid chloride [2, 3, 4] and sulfate baths [5, 6]. There have been few attempts to develop alkaline sulfate baths [7, 8]. To improve the deposit quality and bath stability, triethanolamine and gelatin were added to alkaline baths [9]. To obtain fine-grained zinc-rich deposits, boric acid was added [10]. X-ray diffraction studies on the deposit obtained from an alkaline solution revealed a single η phase, a substitutional solid solution if the zinc content was $>88\%$ [11]. Depending on the current density, the deposition becomes anomalous [12].

Dahms and Croll [13] suggested that the formation of metal hydroxide located in the vicinity of the electrode hindered cobalt deposition. The hydroxides formed "oscillated" under potentiostatic conditions and resulted in nanolaminated structures [14]. On a highly oriented pyrographite, potentiostatic deposition began through the formation of randomly distributed zinc-rich nuclei on the surface, showing an exclusion area around the larger nuclei and preferential nucleation at the kink sites. At long deposition times an incipient dendritic growth related to the initiation of pure cobalt deposition was seen [15]. Potentiodynamic stripping of zinc-cobalt alloy deposits formed on vitreous carbon indicated the initial formation of a cobalt sub-monolayer. Zinc adsorbed on the initial cobalt layer and favoured zinc deposition [16]. In an anodic dissolution of a two-layer Zn-Co alloy coating obtained from a single bath containing Zn^{2+} and Co^{2+} ions, three anodic peaks were seen and were due to the dissolution of pure zinc and of the Zn-Co alloy phase [17].

Experimental

Cold rolled mild steel plates (10×7.5×0.05 cm) were degreased with trichloroethylene and alkaline electrocleaned cathodically for 2 min in a solution of 35 g/L NaOH and 20 g/L Na_2CO_3 at 70 °C. They were washed in running water and dipped in 5% H_2SO_4 solution for 10 s. Finally, they were thoroughly washing with deionized water and dried.

A Hull cell was used to assess and optimize the conditions for the production of good quality deposits. A cell current of 0.5 A was used for a duration of 10 min. A regulated power supply was used as a direct current source and a calibrated ammeter along

K.A. Prasad · P. Giridhar · V. Ravindran
V.S. Muralidharan (✉)
Central Electrochemical Research Institute,
Karaikudi 630006, India
E-mail: corr@cscecri.ren.nic.in

with the cell constituted the electrical circuit. Copper samples were used for the Hull cell experiments. The temperature was kept at 50 ± 1 °C. Electrolytic Zn was used as the anode material. The chemicals used in the preparation of the plating bath were of analytical grade.

Current efficiency studies

For current efficiency (CE) experiments the electrodeposition assembly consisted of an electrolytically pure Zn anode and a steel cathode of equal size (5×4×0.025 cm) immersed in an 800 mL solution in a 1 L wide-mouthed glass vessel. For CE determination, each specimen was weighed before and after deposition and the weight of the deposits was found by difference. The electrodeposits were removed chemically by immersion in 1:1 HNO_3 solution and the solution was analyzed for zinc and cobalt. The amount of cobalt in the deposit was calculated from the difference in the mass of the deposit and that of the zinc determined. The zinc content was determined by atomic absorption spectroscopy (GBC apparatus).

Cyclic voltammetry

Cyclic voltammetry was carried out using a proprietary system (Bioanalytical, model 100A), a conventional three-electrode cell assembly comprising glassy carbon (0.2 cm^2) as the working electrode, platinum as the counter electrode and saturated calomel as the reference electrode. The solutions under study were deoxygenated for 1 h using purified hydrogen. The temperature of the cell was kept at 30 °C; the pH values of the solutions were adjusted using a digital pH meter (± 0.1 accuracy).

The surface of the alloy deposit was analysed for the percentage composition of zinc and cobalt (with ± 1% error) by X-ray fluorescence (CMI, W target). The scanning electron microscope pictures were obtained using a JOEL SEM under various magnifications.

Results

Table 1 presents the compositions and conditions of various Zn-Co alloy plating baths.

Table 1 Compositions of various Zn-Co alloy plating baths

Bath	Ratio of Zn:Co	Composition[a]
A	1:9	0.1 M $ZnSO_4$, 0.9 M $CoSO_4$
B	1:3.6	0.25 M $ZnSO_4$, 0.9 M $CoSO_4$
C	1:2.25	0.4 M $ZnSO_4$, 0.9 M $CoSO_4$
D	1:1.5	0.6 M $ZnSO_4$, 0.9 M $CoSO_4$

[a]Other conditions: 45 g/L NH_4Cl, 0.5 g/L Na_2SO_4, time of deposition 10 min, pH 3–4, temperature 50 °C

Hull cell studies

With an increase in $ZnSO_4$ concentration, the semi-bright deposits obtained in the low current density range disappeared and became brighter. Blackish grey deposits obtained at the higher current density range disappeared. Burnt powdery deposits were seen in 0.6 M $ZnSO_4$ solution. Grey streaky deposits were obtained in the current density range 0.5–1.7 A/dm^2 (Fig. 1).

Current efficiency of alloy deposition

The current efficiency is given by:

$$\%\,\text{Current efficiency} = \frac{\text{Weight of the alloy deposited} \times 100}{\text{Theoretical weight obtained from Faraday's laws}} = \frac{M \times 100}{e_{\text{alloy}} \times Q} \quad (1)$$

where M is the mass of the alloy deposit, Q is the quantity of electricity passed and e_{alloy} is the electrochemical equivalent:

$$e_{\text{alloy}} = \frac{e_{\text{Co}} \times e_{\text{Zn}}}{e_{\text{Co}} f_{\text{Zn}} + e_{\text{Zn}} f_{\text{Co}}} \quad (2)$$

where e_{Co} and e_{Zn} are the electrochemical equivalents of the constituent metals; f_{Co} and f_{Zn} are their fractions in the deposits. The density of the alloy was calculated by taking into consideration the fraction of the constituent metal. Figure 2 presents the variation of current efficiencies with current densities. At all cathode current densities, the CE of the alloy deposition was less than 40%; the CE of zinc deposition was greater than that of cobalt deposition.

Well-known brighteners and leveling agents were used to improve the quality of the deposits. Boric acid (BA), β-naphthol (BN) and sodium lauryl sulfate (SLS) at various concentrations were tried. In order to bring down the cobalt content and retard the hydrogen evolution, various amounts of NH_4Cl were added. The optimum concentration was found to be 45 g/L. Table 2 summarizes the nature of the deposits obtained in the presence of various additives. Grey and uniform deposits were obtained by the addition of BA, SLS and BN in the bath.

Table 3 presents the percentage composition of zinc in the alloy surface and in the bulk of the deposit obtained by XRF and AAS, respectively.

Surface morphology studies

When viewed at ×1500 (Fig. 3a), uniform, spongy small crystallites were seen. With an increase of current density to 1.0 A/dm^2, at a magnification of ×10,000, uniform, nearly spherical < 1 μm crystallites were seen (Fig. 3b). Crystals that became spherical by the agglomeration of the small crystallites covering the surface like a cauliflower were seen at 1.5 A/dm^2 (Fig. 3c). These grains contain packets of hexagonal laminae, each with a pronounced layer structure.

BA and other additives helped in the spreading of already-grown grains (Fig. 3d), resulting in a layered structure. This would not be obtained if BA had not complexed with cobalt. BA seems to affect the nucleation and growth rates. Hexagonal zinc crystals were seen at 1.0 A/dm^2 and, when viewed at higher magnifications, the crystals grown were interconnected by needle-like

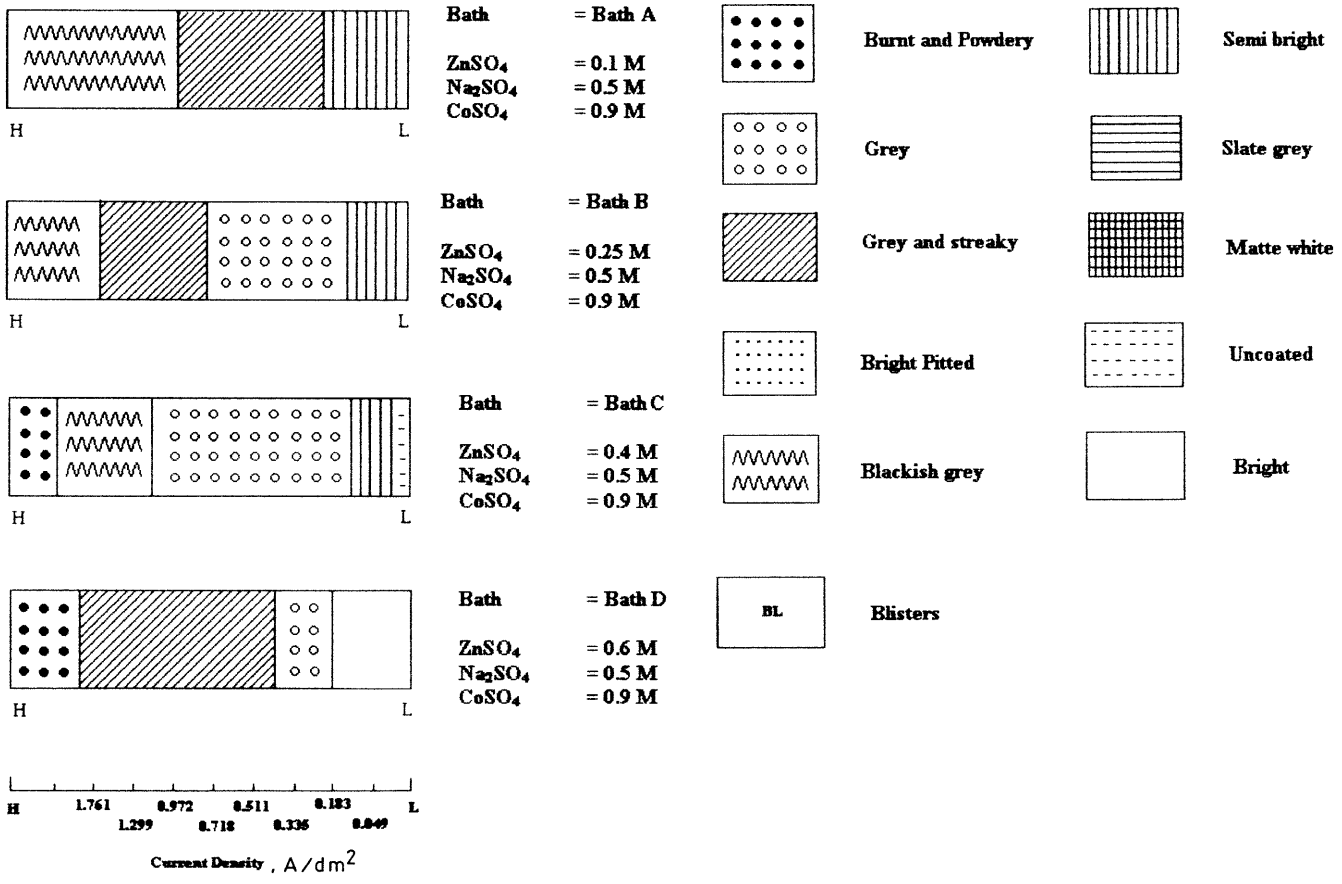

Fig. 1 Hull cell patterns

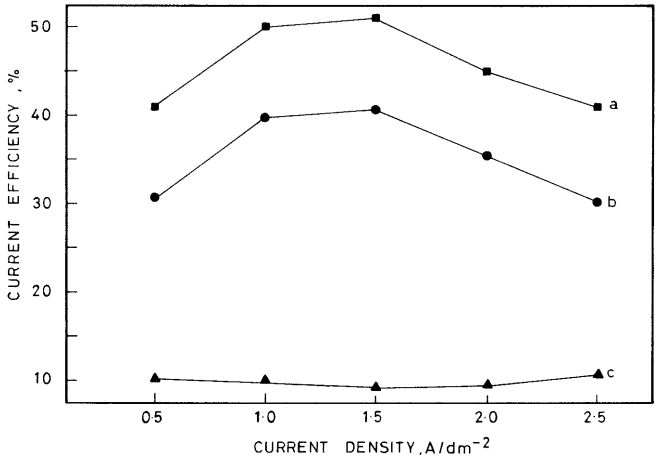

Fig. 2 Variation of current efficiencies with current densities: ■ alloy; ● zinc; ▲ cobalt

particles (Fig. 3e and f). At 1.5 A/dm^2, nearly spherical crystals were seen. Hexagonal crystals of Zn were also seen (Fig. 3g and h). Larger nuclei formed in the secondary nucleation process were due to the growth of the nuclei that were formed in the primary nucleation phase. At these conditions, the growth rate of the nuclei greatly exceeds that of nucleation, resulting in this morphology. The largest nuclei seem to be composed of several large nuclei. In Fig. 3h one may also see the deposits of $ZnCl_2$ on the grown spherical crystallites.

Table 2 Influence of addition agents to the bath D on the nature of the deposit

Addition agent[a]	Nature of deposit
None	Light grey, non-uniform coverage
40 g/L BA	Grey and uniform
0.865 g/L SLS	Light grey, smooth
0.345 g/L BN	Grey, smooth
40 g/L BA + 0.345 g/L BN	Dark grey, patchy
40 g/L BA + 0.865 g/L SLS	Grey, uniform
40 g/L BA + 0.865 g/L SLS + 0.345 g/L BN	Grey, smooth, sparse

[a]Other conditions: temperature 55–60 °C, time of electrodeposition 30 min, current density 0.5 A/dm^2, 45 g/L NH_4Cl, 0.5 M Na_2SO_4; BA, boric acid; BN, β-naphthol; SLS, sodium lauryl sulfate

Cyclic voltammetry

Figure 4 presents the cyclic voltammogram obtained in 0.5 M Na_2SO_4 solutions containing $ZnSO_4$. An excursion of the potential from –1600 mV to –200 mV revealed an anodic peak at –900 mV, while a distinct cathodic peak was seen at –1200 mV in the reverse scan. On repeated cycling the anodic peak potential remained

Table 3 Variation in percentage Zn composition of the deposit with current density

Current density[a] (A/dm^2)	Bulk analysis by AAS (% Zn)	Surface analysis by XRF (% Zn)
0.5	91.5	58
1.0	91.3	70
1.5	78.3	75
2.0	81.4	75
2.5	86.4	75

[a]Bath composition: 0.5 M $ZnSO_4$, 0.5 M $CoSO_4$, 40 g/L BA, 0.865 g/L SLS, 0.345 g/L β-naphthol; other conditions: temperature 55–60 °C, time of electrodeposition 30 min, current density = 0.5 A/dm^2 45 g/L NH_4Cl, 0.5 M Na_2SO_4, pH 3–4

the same while the cathodic peak potentials became more negative, suggesting that the reduction becomes more difficult. The anodic peak potential became nobler with sweep rate (v) and the cathodic peak potential varied with 120 mV/decade change of v. The cathodic peak currents varied with v and $[\mathrm{d}\log i_{p,c}/\mathrm{d}\log v] = 0.33$ was observed. A decade change of $ZnSO_4$ concentration caused the peak currents to vary and $[\mathrm{d}\log i_{p,c}/\mathrm{d}\log(Zn^{2+})]_{pH} = 0.9$.

The cyclic voltammogram obtained in 0.5 M Na_2SO_4 + 0.5 M $CoSO_4$ solution (Fig. 5) revealed, in the forward scan, a broad anodic peak at –300 mV which became nobler with v. The $[\mathrm{d}\log i_{p,c}/\mathrm{d}\log v]_{pH} = 0.5$ and $[\mathrm{d}\log E_{p,a}/\mathrm{d}\log v] = 120$ mV/decade values were obtained.

Figure 6 presents the cyclic voltammogram obtained in 0.5 M Na_2SO_4 + 0.5 M $ZnSO_4$ + 0.5 M $CoSO_4$ solutions. An excursion of the potential from –1300 mV to +400 mV revealed interesting features. Three well-defined anodic peaks appeared at –650 mV (I), –400 mV (II) and –140 mV (III), while the reverse scan exhibited no cathodic peaks. The second cycling caused the anodic peaks to merge after –400 mV. The anodic peak potentials varied as 125, 138 and 62 mV/decade change of v, respectively.

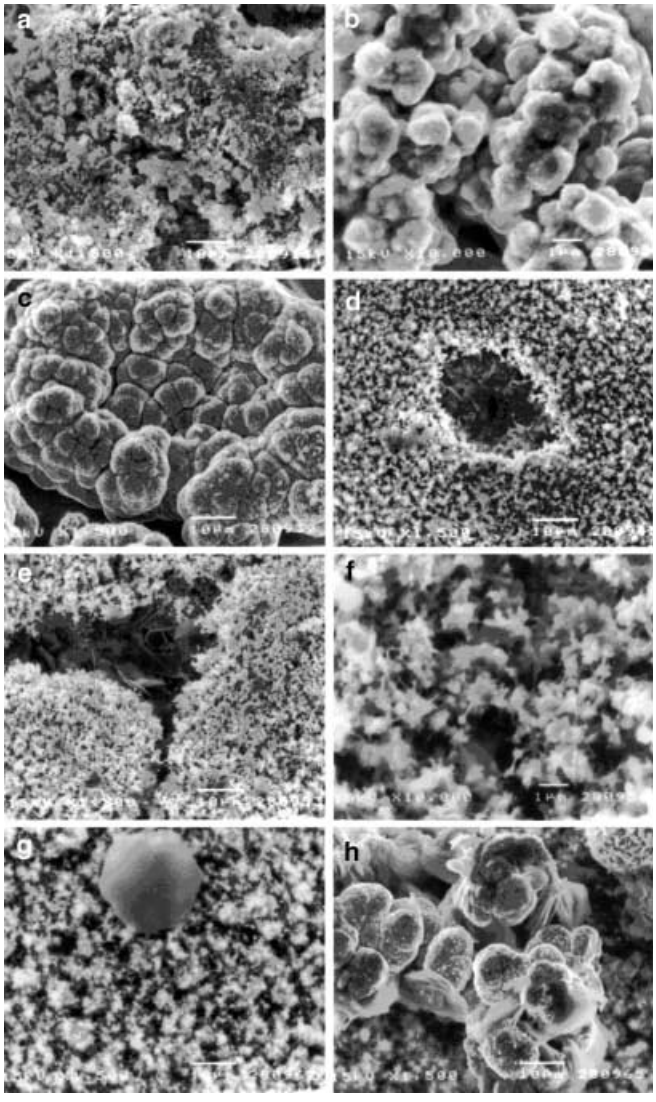

Fig. 3 **a** Scanning electron micrograph obtained for the deposit from the baths without additives at a current density of 0.5 A/dm^2 (×1500). **b** Scanning electron micrograph obtained for the deposit from the baths without additives at a current density of 1.0 A/dm^2 (×10000). **c** Scanning electron micrograph obtained for the deposit from the baths without additives at a current density of 1.5 A/dm^2 (×1500). **d** Scanning electron micrograph obtained for the deposit from the baths in the presence of additives at a current density of 0.5 A/dm^2 (×1500). **e** Scanning electron micrograph obtained for the deposit from the baths in the presence of additives at a current density of 1.0 A/dm^2 (×1500). **f** Scanning electron micrograph obtained for the deposit from the baths in the presence of additives at a current density of 1.0 A/dm^2 (×10,000). **g** Scanning electron micrograph obtained for the deposit from the baths in the presence of additives at a current density of 1.5 A/dm^2 (×1500). **h** Scanning electron micrograph obtained for the deposit from the baths in the presence of additives at a current density of 0.5 A/dm^2 (×1500) at a distant site

Discussion

In $ZnSO_4$ solutions, the deposition of zinc under transient polarization conditions (5–100 mV/s) may involve the formation of Zn^{2+} and:

$$Zn^{2+}_{solution} \longrightarrow Zn^{2+}_{ads} \tag{3}$$

$$Zn^{2+}_{ads} + e^- \longrightarrow Zn^{2+}_{ads} \tag{4}$$

$$Zn^{+}_{ads} + e^- \longrightarrow Zn \tag{5}$$

If the second step is slow:

$$i_c = \overrightarrow{k_2}\overrightarrow{k_1}(Zn^{2+})\exp(-\alpha_c F\Delta\phi_c/RT) \tag{6}$$

where α_c is the cathodic transfer coefficient, $\Delta\phi_c$ is the interfacial potential difference and $\overrightarrow{k_2}\overrightarrow{k_1}$ are the rate constants. If the discharge step is irreversible [18, 19]:

$$E_{p,c} = E^\circ + RT/nF\{\ln k^\circ/\sqrt{D} - 0.5\ln(\alpha F v/RT) - 0.78\} \tag{7}$$

where $E_{p,c}$ is the cathodic peak potential, v is the sweep rate, D is the diffusion coefficient of the Zn^{2+} ions and

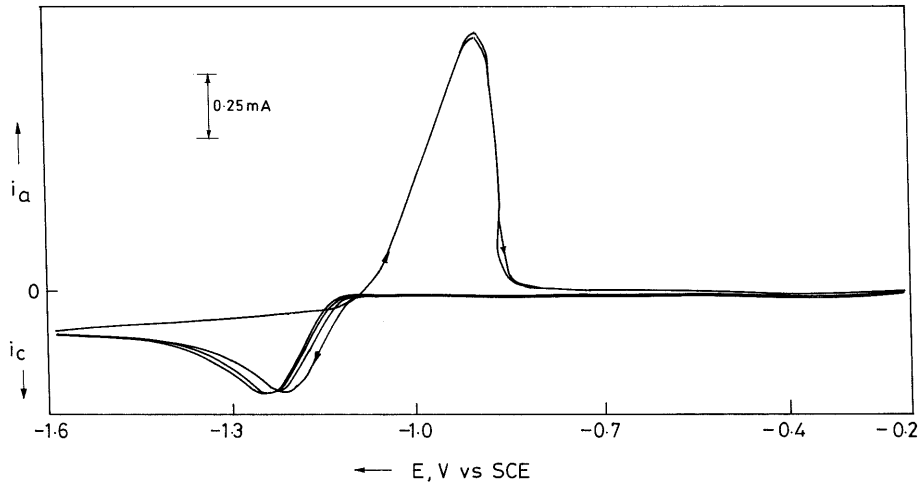

Fig. 4 Typical cyclic voltammogram in 0.5 M Na_2SO_4 + 0.5 M $ZnSO_4$ solutions; $v = 10$ mV/s; $E_{\lambda,c} = -1600$ mV; $E_{\lambda,a} = -200$ mV

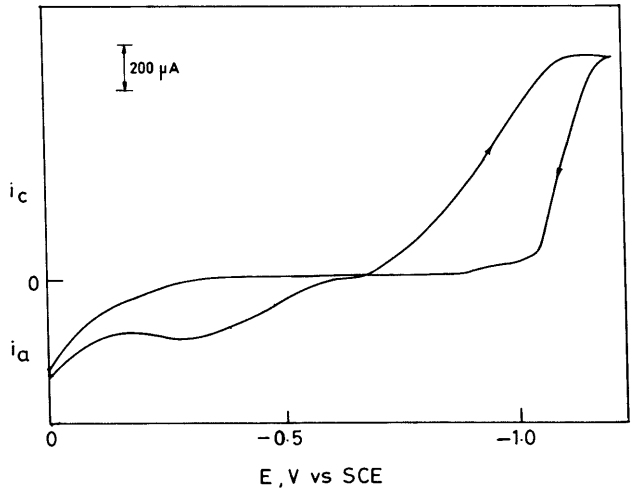

Fig. 5 Typical cyclic voltammogram in 0.5 M Na_2SO_4 + 0.5 M $CoSO_4$ solutions; $v = 10$ mV/s; $E_{\lambda,c} = -1200$ mV; $E_{\lambda,a} = 0$ mV

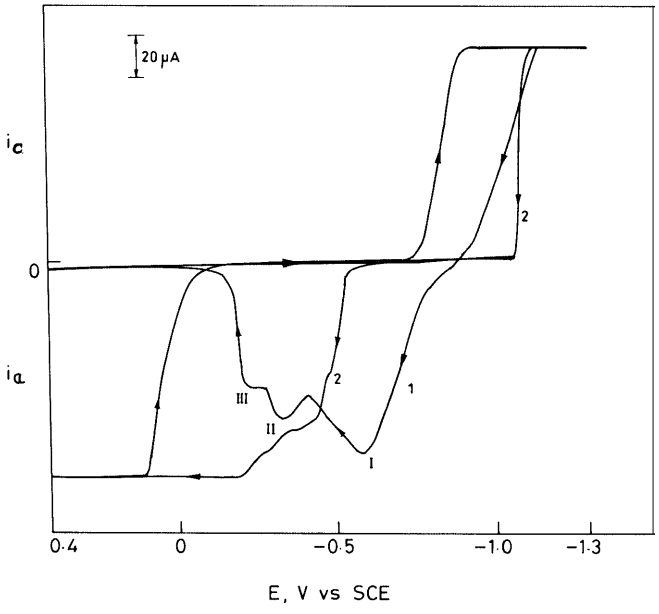

Fig. 6 Typical cyclic voltammogram in 0.5 M Na_2SO_4 + 0.5 M $ZnSO_4$ + 0.5 M $CoSO_4$ solutions; $v = 10$ mV/s; $E_{\lambda,c} = -1300$ mV; $E_{\lambda,a} = 400$ mV

E° is the formal potential. A plot of $E_{p,c}$ vs. log$v$ would give a straight line and the slope would give the cathodic Tafel slope. The observed cathodic Tafel slope of 110 ± 10 mV suggests that the first electron transfer is slow. The dissolution may take place as:

$$Zn \longrightarrow Zn^+_{ads} + e^- \quad \text{(slow)} \tag{8}$$

In cobalt sulfate solutions the electrodeposition of cobalt is accompanied by the generation of OH^- ions. The reverse scan causes the dissolution of deposited cobalt with the formation of monovalent cobalt species:

$$Co + 2OH^- \rightarrow CoOH_{ads} + OH^- + e^- \tag{9}$$

$$CoOH_{ads} \rightleftharpoons CoOH^+_{ads} + e^- \tag{10}$$

$$CoOH^+_{ads} \rightleftharpoons Co^{2+} + OH^- \tag{11}$$

The observed anodic Tafel slope of 120 mV/decade confirms Eq. 9 as a slow step.

Zinc-cobalt alloy deposition

Brenner [12] classified this co-deposition as anomalous because there is a prevailing deposition of the less-noble metal. Fe-Ni, Co-Ni and Zn-Ni alloys are a few other examples of alloy systems which exhibit anomalous behaviour. The deposition of the more-noble metal was suppressed by the preferential deposition of hydroxides of the less-noble metal but not of the more-noble metal. An idea based on the work function was suggested. If the work function of the alloy lies between that of the parent metals, then continuous underpotential of the noble metal is possible. As the electrodeposition is carried out over a prolonged period, it may cause the pH to change near the interface. This would result in the precipitation of the metal hydroxides.

Table 4 Parameters derived from the cyclic voltammogram for zinc dissolution from Zn-Co alloy film at 30 °C, $v = 20$ mV/s

Zn:Co ratio in the solution	$E_{p,a}$ (mV)	Peak intersection potential (mV vs. SCE)	ΔG (kJ mol^{-1})
1:0	–900	–1100	–
0:1	–300	–600	–
1:1	–650	–820	–5.4
	–400	–700	–7.2
	–140	–540	–10.8

Anomalous co-deposition of zinc alloys may be due to:

1. An increase of the surface pH, causing the formation of $Zn(OH)_2$ which may suppress noble metal discharge.
2. Zinc deposition may be controlled by mass transport and noble metal deposition by kinetics.
3. The rate of charge transfer of $ZnOH^+$ or $CoOH^+$ species may be responsible.
4. The monolayer coverage of cobalt may be followed by water molecule chemisorption with the creation of $CoOH^+_{ads}$.

As a result of the competition of zinc and cobalt ions to occupy active sites, the preferential deposition of Zn and suppression of Co discharge takes place. In the present case the difference in the exchange current densities of these metal depositions was found to be the cause of the anomalous deposition [20, 21, 22].

Formation of intermediate species

SEM photographs (Fig. 3g) suggest that large Zn atoms may become trapped on the growing phase, creating distortions and other types of faults in the crystal lattice (which otherwise has no affinity to accommodate them). This phase becomes a supersaturated solid solution or an intermediate phase diagram for the particular composition. The formation of an intermediate or an intermetallic compound can be visualized from the reversible potential of Zn/Zn^{2+} ions in solution. The reversible potential of zinc in a solution of Zn^{2+} ions is:

$$E_r^{Zn} = E_{r,0}^{Zn} + 2.303RT/2F \log\left(a_{Zn^{2+}}/a_{Zn,alloy}\right) \qquad (12)$$

The difference $\Delta E = 2.303RT/2F \log a_{Zn^{2+}}$ and the free energy of alloy formation $\Delta G = -2F\Delta E$.

Table 4 summarizes the results derived from cyclic voltammetric curves for the dissolution of zinc from Zn-Co alloy film. The anodic peaks observed may be due to the presence of different intermetallic compounds or the existence of different crystal structures of zinc in the film. However, considering that the number of peaks depends on the current ratio of the deposition and that the most positive peak (III) of the alloy dissolution is positive by some 600 mV with respect to the reversible potential of zinc, it is unlikely that the three peaks represent the dissolution of three different crystal structures of zinc.

Earlier studies carried out on the dissolution characteristics of Zn-Co alloy deposit of 0.3 μm thickness [22] revealed three anodic peaks at –1300, –1120 and –900 mV and this suggested the existence of not only zinc but also Zn-Co alloys of different content and structures. In the present study the observed large variation in ΔG suggests the existence of three distinct phases rich in zinc or probably corresponding to those of the β, β_1 and γ phases of the Zn-Co alloy [23].

References

1. Verbene WMJC (1986) Trans Inst Met Finish 64:30
2. Short NR et al (1986) Trans Inst Met Finish 64:145
3. Shears (1989) Trans Inst Met Finish 67:67
4. Short NR et al (1989) Trans Inst Met Finish 67:73
5. Higashi K et al (1981) J Electrochem Soc 128:2081
6. Fratesi R, Roventi G (1989) Mater Chem 23:529
7. Kochergin SM, Podebimskii GR (1958) Zh Prikl Khim 31:1432
8. Rajendran S et al (1997) Plating Surf Finish 84:63
9. Narasimhamurthy V, Sheshadri BS (1998) Met Finish (4):24
10. Karawas C, Hepel T (1989) J Electrochem Soc 136:1672
11. Carpenter EOS, Farr JPG (1998) Trans Inst Met Finish 76:135
12. Brenner A (1963) Electrodeposition of alloys, principles and practice. Academic Press, New York
13. Dahms H, Croll IM (1965) J Electrochem Soc 112:771
14. Yan H, Downes J, Boden PJ, Harris SJ (1996) J Electrochem Soc 143:1577
15. Gomez E et al (1995) J Electrochem Soc 142:4091
16. Gomez E, Valles E (1997) J Electroanal Chem 421:157
17. Kirilova I, Nanov I, Rashkov SK (1998) J Appl Electrochem 28:637
18. Nicholson RS, Shain (1964) Anal Chem 36:706
19. Macdonald DD (1977) Transient techniques in electrochemistry. Plenum Press, New York, p 193
20. Aleala M, Gomez E, Valles E (1994) J Electroanal Chem 370:73
21. Mathias M, Chapman T (1987) J Electrochem Soc 134:1408
22. Mathias M, Chapman T (1990) J Electrochem Soc 137:102
23. ASM (1992) ASM handbook, vol 3. Materials Information Society, ASM International, Materials Park, Ohio, p 2.321